Kelechi *et al. J Wireless Com Network (2025) 2026:16*
https://doi.org/10.1186/s13638-025-02499-0

Journal on Wireless Communications and Networking

RESEARCH **Open Access**

Long range battery-free wireless power transfer testbed for underground mines IoT and LPWAN devices

Anabi Hilary Kelechi[1*], Samuel Frimpong[1] and Sanjay Madria[2]

*Correspondence: hav5wv@mst.edu

[1] Department of Mining and Explosives Engineering, Missouri University of Science and Technology, Rolla, MO 65409, USA
[2] Department of Computer Science, Missouri University of Science and Technology, Rolla, MO 65409, USA

Abstract

Underground mines are susceptible to occasional roof falls and cave-ins, temporarily destroying the existing wireless communications and telemetry infrastructure. During this temporary outage, intermittent provision of electrical energy wirelessly to the already deployed low-power wireless area networks (LPWAN) and Internet of Things (IoT) devices assumes a fundamental requirement. In this article, we propose and design a long-range far-field radio frequency (RF) wireless power transfer (WPT) testbed to power LPWAN and IoT devices at 35 m in an underground mines facility. Class AB external power amplifier (PA) was introduced to achieve a long-distance RF WPT, in the 880 MHz band. Thus, considerably reducing the adverse effects of the high signal attenuation power loss of about 50 dB. With the aid of a commercially available off-the-shelf (COTS) TPS61030 boost converter, a 2.5 V/25F supercapacitor was boosted to provide the energy needed to the Heltec ESP32 system-on-chip (SoC) microcontroller unit (MCU). The Heltec ESP32 integrates various components, including a dual-core CPU, LoRa, Wi-Fi, and Bluetooth radio connectivity modules. Thus, realizing far-field, IoT, and LPWAN battery-free technology in underground mines environment. This novel research exploited the concept of utilizing supercapacitors for the storage of harvested energy. To the best of our knowledge, this is the first long-range far-field WPT testbed specifically designed for underground mines facilities at 880 MHz band. In this study, we also investigated the impact of using various modulation schemes. The schemes evaluated were of amplitude modulation (AM), frequency modulation (FM), and pulse width modulation (PWM). Empirical results indicate that the most suitable scheme for RF-WPT in the underground mine is FM. In addition, we performed extensive analysis to understand the energy and current consumption profiles of the Heltec ESP32 LoRa, WiFi, and BLE transceiver using Power Profiler Kit II under different configurations and scenarios. The experimental results indicate that the WiFi connectivity is not energy efficient compared to the BLE transceiver.

Keywords: Low-power wireless area networks (LPWAN), IoT, Wireless power transfer, Underground mines wireless network, Radio frequency energy harvesting (RF-EH), Power amplifier

1 Introduction

The underground mine operations depend on low power wide area network (LPWAN) and Internet of Things (IoT) technology for communication and telemetry services during emergency situations. At present, the energy requirements of these devices depend solely on onboard batteries which are limited in capacity and exorbitant from maintenance point of view. Consequently, there is a need to develop energy self-sustaining IoT and LPWAN devices to drive this ecosystem. Although giant strides have been recorded in the battery life optimization and battery cell efficiency [1] but the battery-free IoT technology is still in infancy stage of development. Radio frequency wireless power transfer (RF-WPT) and energy harvesting (EH) are complementary technologies proposed to drive battery-free IoT and LPWAN processes by providing intermittent or regular energy supply to IoT and LPWAN devices thus, replacing the use of battery to energize IoT and LPWAN devices. Despite the numerous advantages of RF-WPT EH technology, the process is yet to be fully adopted in the IoT and LPWAN ecosystem specifically in underground mine environment [2, 3]. RF-WPT setup has notable issues; i) marginal received signal power by the EH module because of poor RF density per area, ii) short transmitting range of WPT transmitters. The challenge becomes more pronounced in underground mines characterized by highly significant RF signal losses. In addition, empirical studies indicated that, at every 30 meters in the sub-GHz bands, there is an additional 50 dB signal loss in underground mines in comparison with other wireless signal propagation environment [4, 5]. Consequently, to achieve our goal, we built a custom-made high-powered Class AB external power amplifier (PA) transmitter capable of transmitting RF power over a long distance in underground mines.

1.1 Overview of harsh RF underground wireless signal propagation environment

The initial attempt of deploying wireless communication in underground mines dates back to the 1920's [6, 7]. This pioneer study summarized the underground mining wireless environments as: having high RF signal attenuation of about 50 dB comprises of: tilt angle loss, rough surface loss, ore body loss, and grazing angles losses [8, 9]. To validate these claims, measurement campaigns have been conducted and are briefly highlighted. The notable underground mines measurement campaigns that gave these insights includes the 2.4 GHz and 5.8 GHz Canadian Centre for Minerals and Energy Technology (CANMET) experimental mines in Val' d'Or, Canada [10, 11], underground mine gallery of NORCAT Mine, Sudbury, Ontario Canada [12]. A fundamental study on the actual propagation of UHF radio waves in coal mine tunnels were investigated in [4].

In a bid to deploy wireless communications in an underground mining facility, three (3) morphological changes in terms of communication signaling have evolved namely [9], namely: i) through-the-earth (TTE) signaling for extreme-low-frequency (ELF)/ very-low-frequency (VLF)/low-frequency (LF) bands, ii) through-the-wire (TTW) signaling for medium-frequency (MF)/VHF/lower-UHF) (e.g., leaky feeders) bands and, iii) through-the-air (TTA) signaling for upper-UHF/super-high-frequency [10]. Amongst the three methods, TTA is the most deployed and currently adopted by major underground wireless communications equipment vendors such as Becker Mining Systems, MineSite Technology, Mine Radio Systems, MineCom, Tunnel Radio

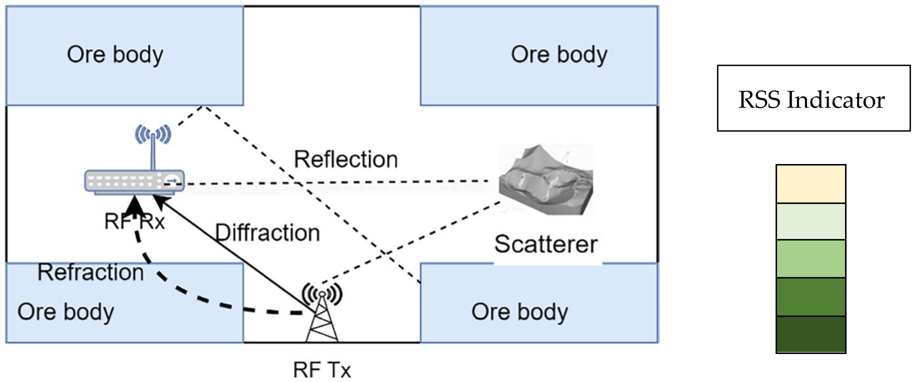

Fig. 1 Wireless signal propagation in normal environments

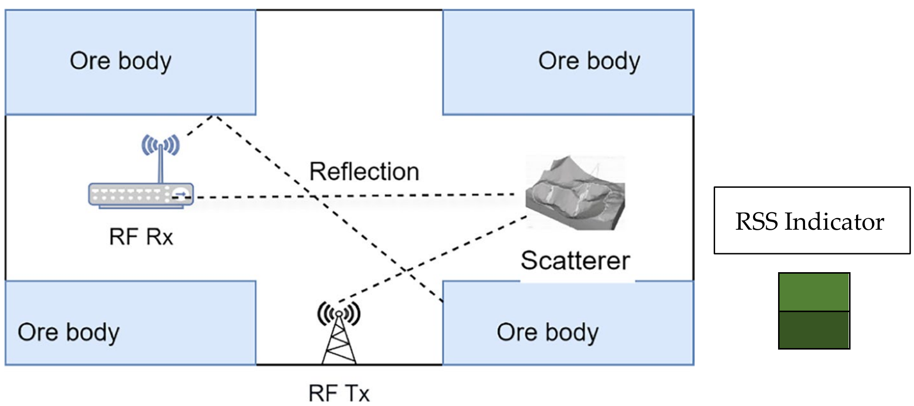

Fig. 2 Underground wireless signal propagation in normal environments

of America and Varis [9]. To ensure the safety of the processes, the National Institute for Occupational Safety and Health (NIOSH) is providing a state-of-the-art technology through regular workshop and tutorials [13, 14].

Evidently, there are severe challenges associated with RF wireless propagation in underground environment as illustrated in Figs. 1 and 2 respectively.

Figure 1 shows that the radio frequency receiver (RF Rx) can receive wireless signals with the aid of reflection, diffraction, and refraction. As a result, the received signal strength indicator (RSSI) is much higher than Fig. 2's value. Explicitly, it is easy to deploy ray tracing technique to estimate the received waveform. Ray tracing is the approximate solution of Maxwell's equation simplified as the sum of free space waveforms from the transmitter plus the reflected free space waveforms from each of the reflecting surfaces. It is assumed that all the various waveform components will add up constructively to boost the received signal or otherwise. In contrast, the underground wireless signal propagation environment as depicted in Fig. 2 can only receive signals via signal reflection. Consequently, there is an absence of wireless channel gains as witnessed earlier, and ray tracing channel model will perform poorly as a modelling tool for underground mines environment. Additionally, there is lack of reflection from ground plain because of the coarse terrain profile of the floor. The

WPT testbeds as currently implemented cannot thrive in underground mining environments considering these unique harsh RF propagation challenges.

Empirical studies conducted previously indicate that the maximum RF-WPT distance is 10 m in a friendly wireless communications environment [15, 16]. Therefore, to achieve long distance RF-WPT in underground mines, a radical approach is required, thus, this is the motivation for this study. Table 1 depicts the already deployed WPT transmitters for RF-EH purposes in their respective environment. Based on the plethora of studies highlighted in Table 1, WPT RF-EH has not been implemented in underground mines environment. Besides, the WPT RF stated distance is very minimal and cannot withstand the harsh RF wireless conditions at the underground mines facilities. More so, the concept of introducing supercapacitors as RF-EH storage devices is yet to be explored despite its numerous advantages. In this study, we explored the use of supercapacitor as a temporary energy storage device for IoT and LPWAN devices.

2 Research contributions

The main innovations and contributions of this article are as follows.

- For the first time, by using commercial off-the-shelf (COTS) components we designed and implemented a far-field long range RF WPT testbed in the 880 MHz band. Specifically, the proposed RF WPT was driven by a class AB power amplifier (PA) capable of radiating RF power to 30 m in a challenging harsh underground mining wireless environment. Several candidate waveform modulation schemes such as Amplitude modulation (AM), Frequency modulation (FM) and Pulse Width modulation (PWM) were investigated. It was discovered that FM square wave performs optimally for WPT. FM, AM and PWM are the most popular radios used in underground mines communication.
- We explored the feasibility of deploying supercapacitors for storing the harvested RF energy. Supercapacitors are endowed with attractive features of fast charging and fast discharging and hence are widely deployed to provide fast burst of energy in an instantaneous time. In this regard, it has gained momentum in electric vehicle (EV) where there is need to constantly supply a rapid burst of energy. Three supercapacitors were considered namely 5 V/1F, 2.5 V/25F and 2.7/100F. The study adopted 2.5 V/25F supercapacitor because it charges faster than the 2.7/100F supercapacitor

Table 1 Various WPT Transmitters Deployed for RF-EH

Authors	WPT Transmitter Type	Radio Frequency Band	Distance	Environment
[3, 15]	PowerCast TX91501	915 MHz, 2.45 GHz	6, 2 m respectively	Measurement Lab
[16]	Universal Software Radio Peripheral (USRP)	915 MHz, 2.45 GHz	1 m, 10 cm	Measurement Lab
[17]	868 MHz ISM-band LoRaWAN radio transceiver	865 MHz	2 m	Measurement Lab
[18]	NI- USRP-2952	2.4 GHz	1 m	Measurement Lab
[19]	USRP B210	868.1 MHz	Not Available	Measurement Lab
[20]	Signal Generator	24 GHz	0.15 m	Measurement Lab
[2]	Agilent E5061B Signal Generator	700 MHz, 850 MHz, 900 MHz	Not Available	Indoor and Outdoor environment

at the expense of storing lesser energy. This study provides the pathway for the realization of battery-free IoT and LPWAN technology.

- Lastly, the 2.5 V/25F was used to energize Heltec ESP32 LoRa WiFi BLE system-on-chip (SoC) microcontroller unit (MCU) thus realizing far-field IoT technology in underground mines facility. The Heltech ESP32 MCU is equipped with three (3) radio transceivers namely: LoRa, WiFi and BLE. to understand the energy and current consumption profiles of the Heltec ESP32 LoRa WiFi and BLE transceiver using Power Profiler Kit II MCU under different configurations.

The rest of the paper is organized as: related work is the focus of Sect. 2. Section 3 discusses the system model of the experiment. The experimental site and testbed description is presented in Sect. 4. An overview of system-on-chip (SoC) microcontroller unit (MCU) was presented in Sect. 5. Lastly, the experimental results and discussion are presented in Section VI.

3 Related studies

The need for an alternative solution to the use of batteries and to deepen the knowledge in RF-WPT has spurred a lot of research in this field. Studies in RF-WPT are categorized into three (3) distinct sub-domains as discussed below.

3.1 RF energy sources

In terms of RF energy sources for WPT purposes, the two (2) dominant sources are: ambient and dedicated RF energy sources. The ambient RF energy source is the RF energy readily available from the ubiquitous radio transmitters. The notable source of this energy includes TV transmitters (Digital/Analog), WiFi access points, satellite transponders, mobile communication transceivers, atmospheric RF energy mainly from lightening and microwave ovens. The ambient RF energy source is characteristically denoted for their weak signal strength. Often, the signal strength is below −30 dBm (100 mW) with a density of 40 $40\mu W/cm^2$ at 10 m and hence, it is very difficult to harvest but not impossible. Most RF-EH modules are functional only at −15 dBm minimum RF signal sensitivity. Under such low sensitivity, RF-EH could be achieved either by designing a single RF-EH tank tuned to a particular frequency or by deploying antenna array with variable impedance matching network. Previous research [21–23] have demonstrated RF-EH with great results using this scheme to harvest RF energy from digital terrestrial TV broadcast and cell towers. Nevertheless, a common observation from ambient RF-EH circuits is that it requires a lot of charge pumps in the form of cascaded circuit to boost the harvested DC power because of the low sensitivity of the received signals and there is a trade-off between power conversion efficiency (PCF) and RF input power [24]. Therefore, the ambient RF-EH is not a reliable source for the underground mining environments, is not a reliable source.

On the other hand, dedicated RF energy sources have found wider acceptance in RF-EH research domains because with these sources, the researcher is at liberty to experiment with different parameters of the transmitter such as transmitter gain [16], waveform end-to-end efficiency [25], and harvested power estimation [26]. Sources of dedicated RF power are listed in Table 1. Dedicated RF energy sources will dominate the scenarios in which there is a lack of ambient RF energy sources such as underground mines, caves, water bodies.

3.2 Efficient radio waveforms

Another school of thought has emerged that analyzed RF-EH efficiency from the perspective of radio waveform designs as discussed within. It is believed that some waveforms perform optimally than others in terms of the RF-EH. The efficiency herein implies the ability of radio waves to yield more DC energy than the others. Digital waveforms have gained traction in RF-EH and are mostly deployed when analog transmit circuits are impractical. Most of the reported works on RF-EH involving digital TV [21, 22], cellular GSM 900, 1800 [23, 27] and cellular 3rd generation network (3G) fall into this category [2]. Digital waveforms are easily simulated by using MATLAB, python scripting language, GNU radio waveform using graphical user interface (GUI) and vector signal generators. Some of the notable works on RF energy harvesting implementing digital communication are LoRa signal [19], OFDM [16] and Bluetooth low energy (BLE) [15]. A study towards choosing the best digital modulation schemes involving phase shift keying (PSK), quadrature amplitude modulation (QAM) and multisine waveforms has been performed [25]. The study concluded that QAM and PSK perform better than the multisine waveforms. Additionally, comparison on the energy efficiency amongst various OFDM subchannels were investigated in [16]. And it was reported that as the number of the subcarriers increases, the amount of RF-EH increases. Most of these studies have deployed software defined radio (SDR) as their testbed of choice. Similarly, with P21XXCSR-EVB EH as the energy harvesting board. The major limitation of the above studies is the deployment of sine wave as the carrier wave. This study practically demonstrates that sine wave is not optimal for energy harvesting because it is a pure wave unlike square, chirp and saw-tooth wave.

3.3 Rectifier/rectenna circuits design

Even after the adoption of P21XXCSR-EVB EH as the RF-EH module of choice by most researchers, substantial works on RF-EH designs are still on-going. For instance, the P21XXCSR-EVB performs optimally at −15 dBm. This implies that any incident wave below this signal threshold sensitivity may not be harvested. To address this issue, [24] proposed and designed a passive RF-DC converter for low RF energy harvesting. The design was able to harvest RF energy at low RF signal of −40 dBm by exploiting many stages of Dickson and Villard voltage multiplier circuits at the expense of RF-DC conversion efficiency. [28] explored the use of multi-path energy routing to improve RF-EH. The impact of receiver antenna orientation of the DC harvested power has also been investigated and reported. The orientation interest was restricted to only 0°–60°. RF energy conversion is actualized using diodes for their passive circuits. Some of the notable diode package models are HMMS-282C, HMMS-285C [22], SMS-7630-079 [29] and Agilent Design Suite (ADS) as the. simulation software. A crucial feature of any selected diode is the threshold voltage. Diodes with lower threshold voltages are desirable because they can harvest RF signals with low sensitivity values and power loss is minimal. To improve the power conversion efficiency (PCE) of RF-EH modules, CMOS technology has been explored.

Unlike diodes that are passive components, i.e., they function in the absence of battery voltages, CMOS technology is more complex. Furthermore, CMOS technology demands longer design and fabrication time which results in expensive chip manufacturing costs. However, the CMOS devices have exhibited high PCE. The notable CMOS technology already deployed are the 130 nm CMOS [30, 31], 90 nm CMOS [32, 33]. Therefore, there is a tradeoff to be considered between CMOS technology and passive diode package models.

4 System model

The goal of RF-WPT in underground mines is to drive energy self-sustaining wireless sensor network (WSN) and IoT thus leading to autonomous network platforms. To achieve this, a system model and overview of solid-state amplifiers are presented in this section.

4.1 Continuous wave RF energy model

The primary design objective of WPT in underground mines is to minimize the high signal attenuation loss from the information carrying wireless signal. Without loss of generality, wireless information carrying signal E_{dBm} can be modeled as:

$$E_{dBm} = Asin\left(2\pi ft + \emptyset\right) \tag{1}$$

A is the baseband signal RF amplitude, sin is the RF carrier wave, ft is the time dependent signaling frequency and $\varnothing$ is the signal phase angle. The signal phase is responsible for the delay caused by the radiation travelling at the speed of the light. The carrier waveform is not only restricted to sine wave. Other carrier waveforms are also possible namely: cos, square, triangle, ramp waves. The information carrying signal has maximum power when the value of the amplitude waveform is unity. From the hardware circuitry perspective, the information carrying signal can be generated via a signal generator with suitable AC voltage (V) stated as:

$$V_{Peak} = \frac{V_{pp}}{2} \tag{2}$$

V_{Peak} is the peak AC voltage generated from the signal generator and V_{pp} is the signal generator peak-to-peak AC voltage. The root-mean-square voltage V_{RMS} is desirable and can be generated as:

$$V_{RMS} = \frac{V_{Peak}}{\sqrt{2}} \tag{3}$$

The signal power (P) passing through a standard voltage 50Ω antenna port impedance is calculated as:

$$P = \frac{V_{RMS}^2}{50\Omega} \tag{4}$$

Then, the power in dBm:

$$P_{dBm} = 20\log_{10}\left(\frac{P}{1mw}\right) \quad (5)$$

Equation (5) simply implies that it is this AC power transmitted over the antenna that we intend to harvest and convert to DC power. For instance, the V_{RMS}^2 required to generate 0 dBm of power is 223 mV. The information carrying signal is modulated using any of the common type of modulation schemes as shown in Fig. 3.

4.2 Far-field RF WPT-EH modeling for underground mines

The building block of far-field RF WPT-EH modeling is based on free space model. In the far-field, the electric field and the magnetic field at any given direction is perpendicular to the another and to the direction of propagation of the transmitting antenna. Note, we can re-write Eq. (1) as $\cos 2\pi f(t - r/c)$; r is the separation distance between the transmitter and the receiver,$c = 3 \times 10^8 m/s$ is the speed of light in vacuum. The received waveform in free space in the absence of pathloss in an electric far field at location **u** at time t is stated as [34]:

$$E_r(f, t, (r, \theta, \varphi)) = \frac{\alpha(\theta, \varphi, f)\cos 2\pi f(t - r/c)}{r} \quad (6)$$

where, (r, θ, φ) denotes location **u** in the space at which the electric field is being measured, (θ, φ) denotes the vertical and horizontal angles from the antenna to point **u**. $\alpha(\theta, \varphi, f)$ signifies the product of the radiation pattern of the transmitting and receiving antennas at frequency f in the given direction of (θ, φ); it also contains scaling factor which accounts for antenna losses. It should be observed that the phase of the electric field varies with fr/c. It could be seen that as distance increases, the electric field strength decreases as r^{-1} and the power as square meter in free space wave decreases by r^{-2}. Next, the received power P_R at the antenna receiver deployed in an underground facility can be modeled as:

$$P_R = G_T G_R \left(\frac{\lambda}{4\pi r}\right)^2 P_{dBm} \quad (7)$$

G_T is the gain of the RF energy transmitter, G_R is the gain of the antenna attached to the Powercast P21XXCSR-EVB RF power harvester, λ is the signal wavelength. Due

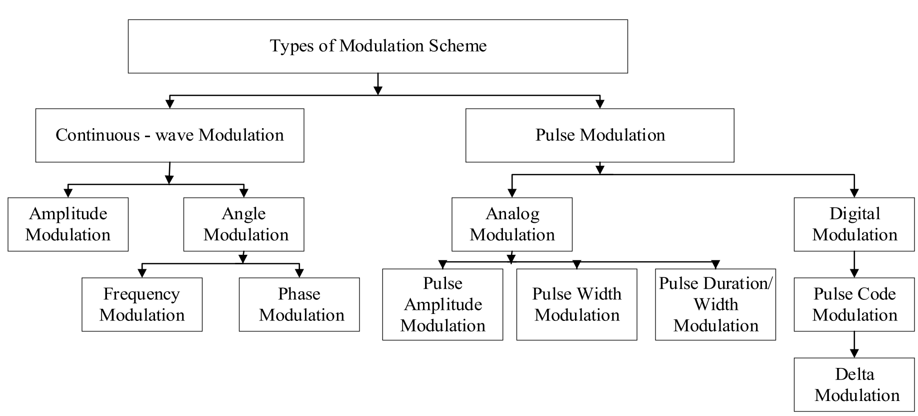

Fig. 3 Types of modulation schemes

to the high RF signal loss in the underground mines, the signals generated in Eq. (5) is worthless from the perspective of RF-EH. It is lacking sufficient RF power, and it is not possible to generate DC power at underground mines facility. Thus, there is need to extend Eq. (5) to encompass external PA component and thus, derive the total transmitted power P_{Total} expressed in logarithmic scale as:

$$P_{Total} = P_{dBm} + P_{PA} \tag{8}$$

P_{PA} is the power of the external PA measured in dBm influenced by the gain of the PA. The three important performance parameters for the PA are the gain, the power ratings and power efficiency explained shortly. Hence, the received power at the antenna receiver is stated as:

$$P_R = G_T G_R \left(\frac{\lambda}{4\pi r}\right)^2 P_{Total} \tag{9}$$

The free space pathloss $L_P(dBm)$ between the transmitting antenna and the Powercast P21XXCSR-EVB is stated as [22]:

$$L_P(dBm) = 32.4 + 20 \times log(f) + 20log(r) \tag{10}$$

In the absence of empirical pathloss model for underground mines, the received power on a logarithmic scale is:

$$P_R(dB) = P_{Total} + G_T + G_R - L_P = EIRP - L_P \tag{11}$$

Finally, the received power of an RF-EH module in the presence of pathloss measurement is stated as:

$$P_R(dB) = EIRP - L_{Pmine} \tag{12}$$

L_{Pmine} is the underground mines facility specific pathloss calculated in decibels. Note, the goal of this study inot to empirically determine the pathloss at underground mines as numerous studies have already performed extensive research on this topic as highlighted earlier. Therefore, RF-EH is feasible in the following conditions:

$$P_R(r,t) = \begin{cases} EIRP - L_{P\,\min e} & > P_{sen}^{\min} \\ 0 & Otherwise \end{cases} \tag{13}$$

Equation (13) implies that if the received power at a distance in an instantaneous time $P_R(r,t)$ is less than the minimum RE-EH sensitivity P_{sen}^{min}, then RF-EH is harvesting is not feasible. Different RF-EH modules have various sensitivity values ranging from – 11 dBm to – 30 dBm [35].

4.3 Solid state amplifier: overview

The success of RF-EH in underground mines depends solely on the solid-state amplifiers deployed. Important attributes of ideal amplifiers are linearity, signal gain, efficiency, in-band parasitic frequencies (3d IM products), out-band parasitic frequencies and power output. However, in real world deployment scenario, there is always a tradeoff in these attributes depending on the underlying applications. Furthermore, amplifier classes are also a key indicator on how the input signal varies in an amplifier circuit when a sinusoidal signal is applied. The main classes of amplifier are class A, B, AB, and C.

i. Class A amplifier: This is a special class of amplifiers with high fidelity at the expense of low efficiency. Unlike other classes of amplifier, class A amplifier uses only one (1) switching transistor (Bipolar, FET, IGBT, etc.) in its output design. For optimal operation of a class A amplifier, it is biased around the Q-point which is the middle line between its load line. Hence, it is never driven into the cut-off or saturation regions. This makes it possible for the current to conduct over the full 360 degrees of the input circle. Unfortunately, this amplifier never turns off and it is not power efficient [36]. It is widely deployed for audio signals.
ii. Class B amplifier: Class B amplifier offers high improvement in terms of power consumption efficiency over class A amplifier. There is no DC base bias current involved because the quiescent current is zero resulting in little DC power consumption. The amplifier sacrifices linearity over low power consumption. Secondly, the amplifier suffers from crossover distortion problems. Unlike the previous class A amplifier, which uses a single switching transistor in its output design, class B design deploys two (2) complementary transistors in a push–pull design configuration. This implies that each transistor amplifies only half of the output waveform [37].
iii. Class AB amplifier: Class AB amplifier combines the attractive qualities of both class A and class B amplifiers to offer a better service than either of them. It has a midrange conduction band, and it should be noted that this amplifier introduces diodes in its design to eliminate the crossover distortion problem inherent in class B amplifier. The diodes supply the transistors with small bias voltage enabling each of the transistors to conduct slightly more than the conduction cycle of class B amplifier. Class AB amplifiers offers higher power efficiency and linearity when compared with class A and class B amplifiers respectively [38].
iv. Class C amplifier: This class of amplifier offers the greatest efficiency of about 80% at the expense of linearity. The other amplifiers are generally classified as linear amplifiers because the output response is directly related to the input trigger. In contrast to other amplifiers, class C amplifier is heavily biased so that the output current is zero for more than one half of an input sinusoidal signal cycle with the transistor idling at its cut-off point[39]. It is difficult to implement because it is designed using tuned circuits.

5 Methods/experimental

This experiment was performed at underground mining gallery and Missouri S&T's Experimental Mines located at Rolla, Missouri in the United States of America.

5.1 The design of the study: underground mines gallery

The underground mines were previously used to mine limestone and dolomite before it was abandoned and subsequently deployed for experimental and training purposes. The section of the underground mining gallery layout used in this experiment is highlighted

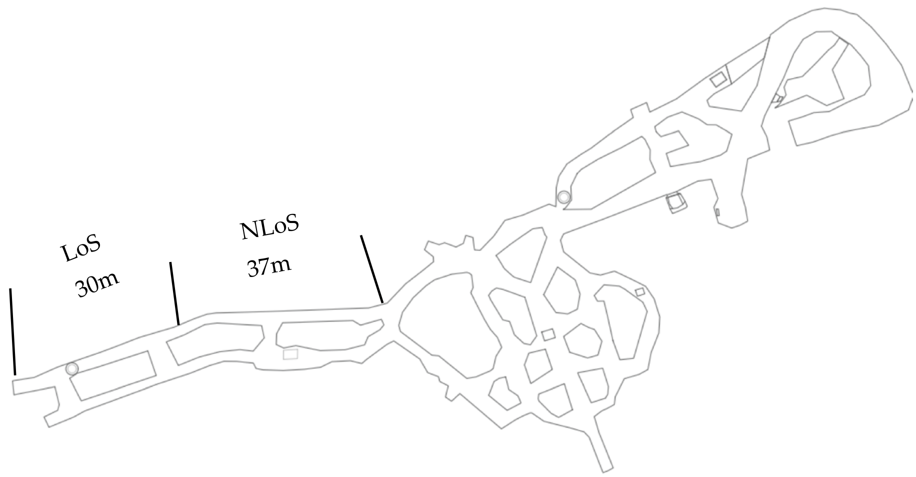

Fig. 4 The mine gallery

Table 2 Utilized hardware and software device/software function

Laptop	HP Intel(R) Core (TM) i5-1035G1 CPU @ 1.00 GHz 1.19 GHz, Windows 10
Vector signal generator	VSG60A 6 GHz—Signal Hound, VSG60 Signal Generation Software
Transmit antenna	880–960 MHz high gain directional 11 dBi Yagi
Receiver antenna	VERT900 vertical antenna omnidirectional, gain 3 dBi
WPT receiver	Powercast P21XXCSR-EVB
Power amplifiers (PAs)	880–960 MHz, 35Watt; 860–960 MHz, 18 Watt; 500–1200 MHz, 80 Watt
Oscilloscope	KEYSIGHT DSOX1204A, Keysight PathWave BenchVue App
Connectors	Laptop to VSG60A: USB2.0, VSG60A to PAs: SMA plug male pin To SMA plug male connector -TNC male connector, WPT receiver to Oscilloscope: jumper cables
DC power supply	30 V/10A DC

in Fig. 4. The layout has rough surfaces, very high humidity, adjacent layouts, and tilted walls. Additionally, the layouts ceilings are flatter than the floor and have some water sumps. The total length of the section used was 67 meters comprising 30 meters line of sight (LoS) and 37 meters non-line of sight (NLoS). The dimensions of the underground mining drift include a width of 2.5 meters, height of 2.2 meters, depth of 10 meters.

5.2 The experimental settings: testbed design transmitter side

In this subsection, we describe the RF-EH testbed specifically the transmitter side. While Table 2 illustrates some of the major hardware and software components of the testbed. Figure 5 depicts the overall testbed deployed in the underground mining facility. The testbed chain mainly of vector signal generator hardware (VSG60A), the VSG60A software interface installed on a laptop, external power amplifier mounted on a heatsink, a high directional antenna and a 30V/10A DC power supply.

i. Equipment Description: Vector Signal Generator Hardware (VSG60A).

The vector signal generator hardware is the Signal Hound VSG60A. It covers RF range of 50 MHz to 6 GHz with a spectrum bandwidth of 40 MHz [40, 41].This particular

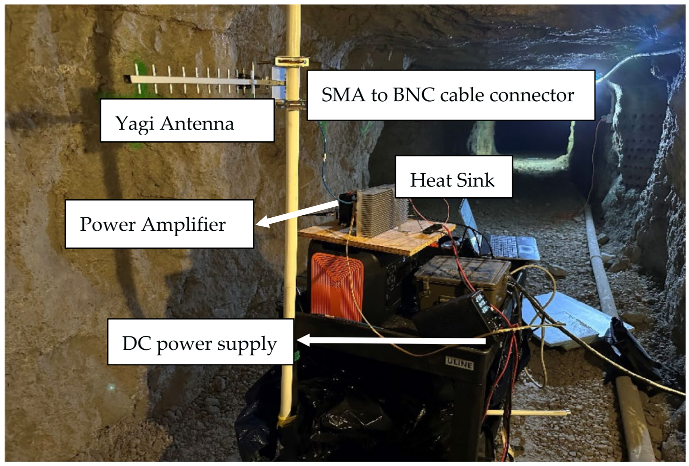

Fig. 5 The proposed long-range WPT testbed

device has been gaining momentum recently in waveform generator as could be seen in [42, 43]. Of particular interest is its ability to generate arbitrary in-phase/ quadrature (I/Q) samples. The I/Q sample rate is from 12.5 kSPS to 51.2 MSPS including 30.72 MSPS for LTE.

ii. Equipment Description: VSG60A Software Interface.

The VSG60A is connected to the computer via the USB 3.0 to display the interface. The software can run smoothly on Windows 10 (32/64-bit) and Ubuntu 18.04 (64-bit). The device comes with some preprogrammed modulation schemes namely: OFDM, LTE, AM, FM, Bluetooth LE, QAM, PSK, CW, IEEE 802.11 a-ax etc. Evidently, the VSG60A can generate a variety of different RF signals and thus satisfy any waveform requirement.

iii. Power Amplifiers.

Since VSG60A is typically a baseband generator lacking any inbuilt signal amplifier, there is a need to incorporate some external PAs. For this study, we experiment with three (3) classes of high PAs from different vendors specifically:

Type I, Max 12.6 DC Volts/7A.

860–960 MHz, 35Watt RF power output, 26 dB Gain, class AB amplifier.

Type II,12 DC Volts/3.3A.

860–960 MHz, 18Watt RF power output, 42 dB Gain, class AB amplifier.

Class B, Max 28 DC Volts/7A.

500–1200 MHz, 80Watt RF power output, 23 dB Gain, class B amplifier.

The role of the PAs is to enhance and amplify the weak signal from the VSG60A which operates at a dynamic range of −55 dBm to +7 dBm excluding the cable losses. The PAs are biased using an external 30V/10A DC power supply. Type I and Type II are indicators to distinguish the two (2) class AB PAs used in this work.

iv) High Gain RF Antenna

Antennas play a crucial role in RF signal propagation. The higher the directivity of an antenna, the higher the gain and vice-versa [44, 45]. Based on this, we experimented with one (1) type of commercially available 880–960 MHz high gain directional 11 dBi, Yagi antenna and which can be either vertically or horizontally polarized. For this study, we deployed vertical polarization. Extra care was taken to align the transmitter and receiver to reduce system performance loss that will arise because of misalignment. The WPT receiver side comprises P21XX PowerHarvester, and digital signal oscilloscope as shown in Fig. 6.

5.3 Receiver side: powercast P21XXCSR-EVB

P21XXPowerharvester® Chipset Reference Design Evaluation Board [46] . It harvests RF energy from the testbed and converts it to DC voltage which can be utilized to power some low energy sensors. e device is capable of harvesting RF energy sources at the following frequencies: 836.5 MHz, 879.5 MHz, 904 MHz, 1747.5 MHz, 1880 MHz and 2450 MHz. These frequencies cover GSM-850 uplink, Europe RFID and GSM-850 downlink, ISM USA and GSM-900 uplink, GSM-1800 uplink, GSM-1900 uplink and WiFi-2.4 GHz. The P21XXPowerharvester® Chipset Reference Design Evaluation Board has an inbuilt LED load which only comes up in the presence of DC voltage. Table 3 summarizes the key specifications of P21XXPowerharvester® Chipset Reference Design Evaluation Board components.

6 ESP32 micro controller unit: overview

Since the ESP32 boards are the major drivers of IoT technology owning to the numerous kernels linking the various sensory peripherals over the Internet protocol, it is important to discuss one of the numerous ESP32 Dev Boards. In this study, we adopted Heltec ESP32 SoC Dev Board. The board is equipped with three (3) radio connectivity modules namely Bluetooth Low Energy (BLE) 5.0, Wi-Fi and Long Range (LoRa) radios respectively.

6.1 Basic functional blocks of ESP32 MCU system-on-chip

The ESP32 SoC MCU mainly consists of various modules, including a dual-core central processing unit (CPU), Wi-Fi and Bluetooth wireless transceivers, numerous peripherals (e.g., GPIO, ADC, PWM), and an ultra-low power coprocessor (ULP) as depicted in Fig. 7. There are also provisions for security components like secure boot and flash encryption features. The ESP32 SoC MCU can operate in four (4) main power modes namely: i) active; ii) modem sleep (ESP32 Light Sleep); iii) deep sleep and iv) hibernation

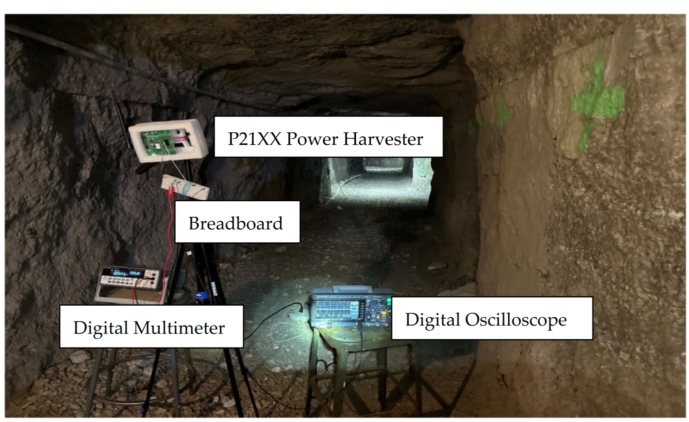

Fig. 6 WPT receiver side

Table 3 P21XXPowerharvester description

Component	Function
J1–J6	These are antenna ports for selecting the various RF bands 836.5–2450 MHz antenna input
JP1	This is a switch for selecting the capacitor to store the harvested voltage
C1–C3	Capacitors for storing harvested voltage. C2 is user defined capacitor
JP2	Jumper which must align with the selected antenna port. Since the device does not implement a diplexer, only one RF band will be harvested at a time
JP3–JP5	These are jumpers indicating the various DC voltages that can be obtained after RF-DC conversion. The DC voltages are 1.2 V, 0.9 V and 0.7 V respectively
S1	S1 is a switch for selecting various output voltages from the boost converter. The boost converter can generate 3.3 V, 4.2–4.1 V or even 5 V
S2	This is a switch for selecting DSET and DOUT which are terminals for measuring the received signal strength indicator (RSSI) after conversion
S3	Controls the selection of the LED which indicates the presence of DC power and VOUT and GND terminals for measuring the harvested DC voltage by selecting the MEAS/VCC button
VCAP	This is used to measure the harvested energy stored in the capacitor

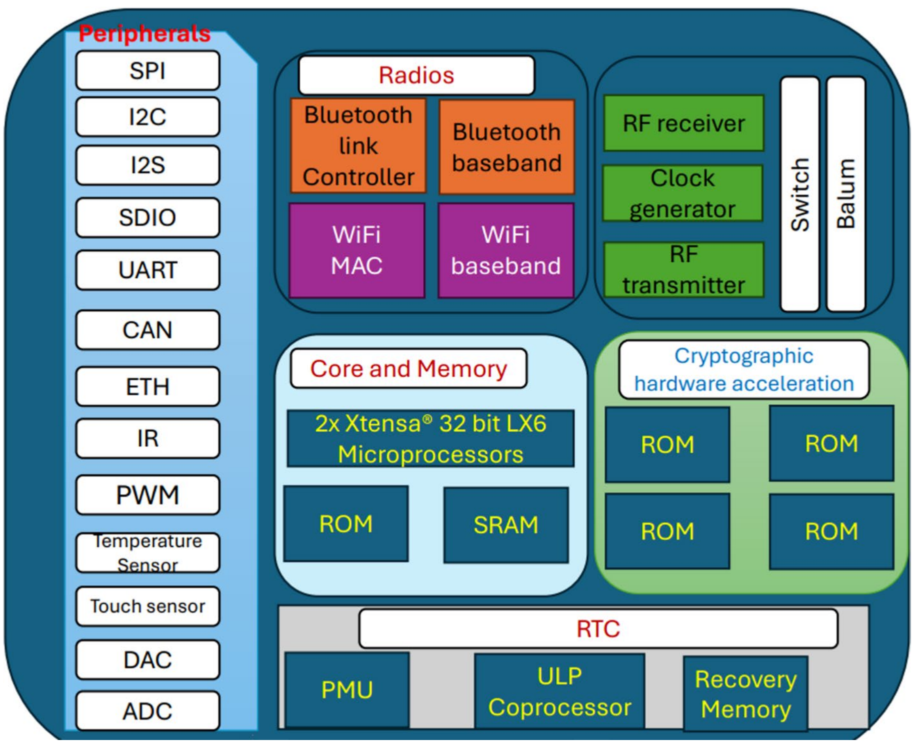

Fig. 7 ESP32 SoC MCU

modes. In active mode, all the six (6) modules of the ESP32 SoC MCU are operating maximally. In this mode, the energy consumption of the ESP32 SoC MCU is at its maximum. The modem sleep or light sleep mode involves shutting down the radio transceiver modules while waiting for an external trigger such as sensor data or external stimulus. This implies that there are no underlying RF functions momentarily ongoing. The deep sleep involves shutting down the main ESP32 core, which includes main processing power and memory, resulting in minimal power usage. With this configuration, the ULP coprocessor is the only active module. The ESP32 SoC MCU waits for an external trigger or timer to wake up from deep sleep. Lastly, hibernation is the most power-efficient mode. It's useful for ultra-low power applications with long sleep periods, such as remote sensor nodes running on batteries and supercapacitors.

i. ESP32 Core CPU and Memory.

This is the main processor of the chip, integrated with memory. The key components in this part are microprocessor, cache, static random-access memory (SRAM), joint test action group (JTAG) and read-only memory (ROM). The ESP32 core CPU and memory are responsible for undertaking the heavy computational functions of the chip and managing other subunits of the ESP32 MCU SoC.

ii. Radios.

The radio connectivity comprises of several transmitters and receivers designed to function within the SoC architecture. The module is responsible for the wireless communications functionality of any SoC MCU module. This ESP32 SoC MCU is equipped with Wi-Fi, BLE 5.0 and LoRa modules. For this study, our focus is on BLE and Wi-Fi radio connectivity because both are widely deployed for IoT and LPWAN applications.

iii. ULP Coprocessor.

The ultra-low power (ULP) is a dedicated microcontroller core constructed to effectively manage low-power and sensory tasks while the main CPU core is in deep sleep mode. ULP includes various key components, such as ULP CPU core, memory, sensor interface, timers, wake-up capabilities.

iv. Real Time Clock.

The real time clock (RTC) module is responsible for providing precise timekeeping and time-associated tasks. The RTC is specifically designed to monitor time, execute time-based procedures, and schedule wake-up events. It comprises some of the key components, such as RTC memory, power management unit (PMU) and brownout detector.

v. Peripherals.

The peripherals consist of numerous hardware interfaces on the chip permitting the integration of the core with sensors, external devices, and many more. Some of the main peripherals are UART, USB On-The-Go (USB OTG), RMT, system timer, pulse counter, LED PWM, LCD interface, I2S, I2C, camera interface, GPIO, USB Serial/JTAG and more.

6.2 Heltec ESP32 LoRa WiFi BLE development board

The Heltec ESP32 SoC is a classic IoT dev-board designed and produced by Heltec Automation. Since its launch in 2017, it has garnered widespread attention by IoT developers and hobbyists. The newly launched V3 version has the same pin sequence as the V2 version and retains Wi-Fi, BLE, LoRa, OLED display, and other functions [47]. The main features of this ESP32 SoC MCU:

- Microprocessor: ESP32-S3FN8 (Xtensa® 32-bit LX7 dual-core processor, five-stage pipeline rack structure, frequency up to 240 MHz).
- SX1262 LoRa node chip.
- Type-C USB interface with a complete voltage regulator, ESD protection, short circuit protection, RF shielding, and other protection measures.

- Onboard SH1.25–2 battery interface, integrated lithium battery management system (charge and discharge management, overcharge protection, battery power detection, USB / battery power automatic switching).
- Onboard 0.96-inch 128 × 64 dot matrix OLED display can be used to display debugging information, battery power, and other relevant information.
- Integrated WiFi, LoRa, Bluetooth three network connections, onboard Wi-Fi, Bluetooth dedicated 2.4 GHz metal spring antenna, reserved IPEX (U.FL) interface for LoRa use.
- Integrated CP2102 USB to serial port chip, convenient for program downloading, and debugging information printing.
- Support the Arduino development environment.
- Startup voltage is 3.7 V.

7 Results and discussions

Some selected experimental results obtained from the experimental setup are presented and discussed. The parameter settings used in this experiment are presented in Table 4. The result of the harvested energy involving the three (3) different types of modulation schemes namely AM, FM and PWM is presented. Furthermore, we also present the results of using different carrier waves. We chose the best modulation scheme to charge the 2.5V/25F supercapacitor which was eventually deployed to power the Heltec ESP32 SoC MCU. Using the 2.5V/25F supercapacitor, we analyze the energy, power and current consumption of the Heltec ESP32 SoC MCU.

7.1 Comparison between the different classes of PAs

Here, we analyze the performance of the three (3) different PAs deployed in this study as derived from Equ. (8). The PAs can operate from 830 to 880 MHz. Environmental factors such as underground material properties (e.g., rock conductivity, humidity) weren't considered in the study because the impacts of rock conductivity and humidity are well documented in underground mines environment. Additionally, rock conductivity, both thermal and electrical, is a complex property influenced by factors like mineral composition, porosity, pore water properties, and temperature. The goal of this analysis is to determine which of the PAs yields the maximum distance from the context of WPT. The RF power from the VSG60A interface was set to 10 dBm. Since it is obvious that higher transmit, power will lead to higher WPT range. From the P21XXPowerharvester

Table 4 Experimental parameter variables

Modulation scheme	Carrier wave	Duty cycle (%)	RF power (dBm)	Radio frequency (MHz)	Power amplifier
AM	Sine, Square, Ramp, Triangle	None	0, 10	880	Class AB Type I, Class AB Type II, Class B
FM	Sine, Square, Ramp, Triangle	None	0, 10	880	Class AB Type I, Class AB Type II, Class B
PWM	Square	25, 50, 75, 100	0, 10	880	Class AB Type I, Class AB Type II, Class B

receiver side, we alternate the jumpers between J1 and J2 to correspond to the RF band under investigation. The JP3 was left at 1.2 Volts. The S1 was set at 4.1–4.2 Volts because we intended to store the harvested DC energy on a supercapacitor. Moreover, the higher the DC voltage, the faster the supercapacitor charging rate. Finally, S3 was selected to measure the harvested DC voltage between the VOUT and GND terminals by selecting the MEAS/VCC button. Note during this phase, no load i.e. MCU has been connected and the supercapacitor is not charging yet. Figure 8 shows the WPT over some distance.

From the graph, Class AB Type I delivers the farthest distance of about 40 m at 880 MHz band. Even though Class B amplifier is of a higher RF power, it performed poorly in comparison to Class AB Type I. Thus, supporting the notion that Class B PA is not power efficient. This shows that the future of RF energy harvesting lies in Class AB amplifier despite its RF power ratings. There are several types of carrier waves investigated in the study including square, sine, triangular and cosine waves. FM and AM are both modulation schemes and are not considered as carrier waves. The major limitation of using supercapacitor is the self- discharge issue which is also common with Lithium-ion batteries. It was observed that in extreme cold conditions, the supercapacitor performance becomes chaotic because of the non-movement of the electrons and vice versa. For insights into the self-discharge suppression of electrochemical capacitors progress and challenges, see [48]

7.2 Performance of AM, FM carrier waveform

Figure 9 depicts the DC voltage when VSG60A interface was set to 10 dBm derived from Equ. (5), and different carrier waveforms are experimented with. Evidently, FM square carrier wave yields optimal result from a distance perspective while the ramp carrier wave is the least attractive waveform for WPT. Hence, there is consistency in FM modulation being better long-range EH-WPT candidate than AM modulation. Additionally, square carrier wave outperforms other carrier waves studied because it consists of several harmonics of the fundamental frequency. The frequency spectrum of square wave consists of fundamental frequency and series of odd integer harmonics which reduce in

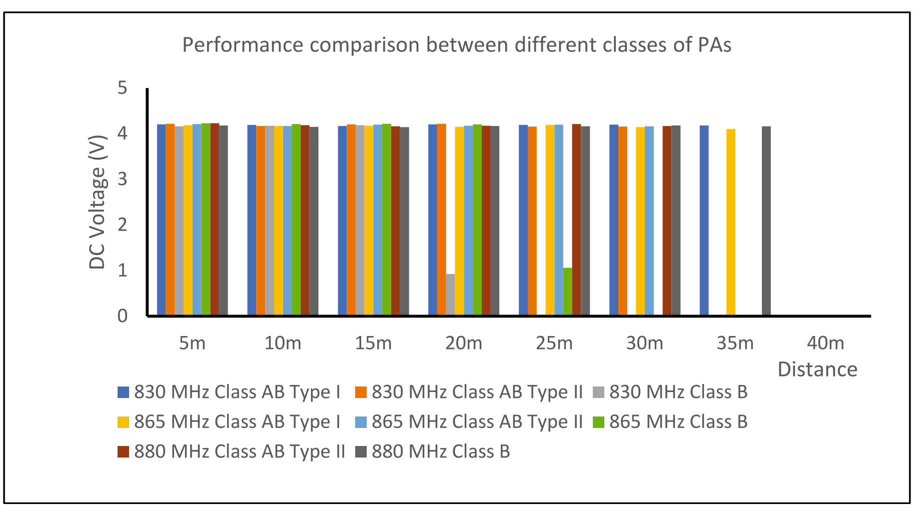

Fig. 8 Performance comparison between different PAs

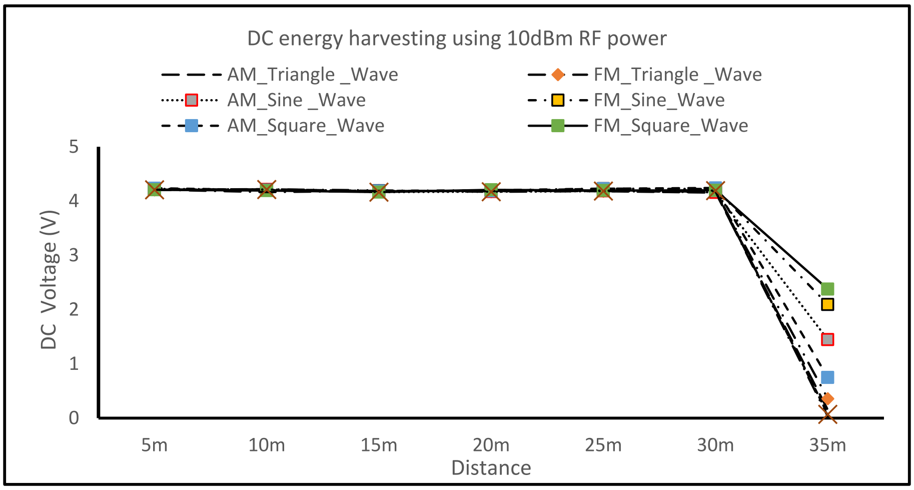

Fig. 9 AM, FM DC voltage over distance with 10dBm RF power

amplitude as frequency increases. This implies that the future of EH-WPT will be centered around FM square carrier waveform.

7.3 Performance of PWM different duty cycle

Leaving the parameter settings unchanged from the WPT P21XXPowerharvester receiver side, we study the harvestable energy based on different PWM duty cycles of 25%, 50%, 75% and 100% respectively. Figure 10 depicts the DC voltage across a wide spectrum of PWM duty cycles. Clearly, the 100% duty cycle yields the maximum range of 30 m. In the 100% duty cycle, the RF chains in the modulator are continuously transmitted. Hence, the reason for the longer distance.

7.4 Performance comparision between AM, FM and PWM

We extended our analyses by comparing the AM, FM or PWM modulation schemes at 880 MHz frequency band. Since most radios currently deploy in underground mines are based on either AM, FM or PWM. One of the main motivations for this study is to decipher the most attractive modulation scheme from the WPT range context. Figure 11 illustrates that the FM modulation scheme yields the farthest harvestable DC WPT at 35 m when 10dBm RF power was selected. The least range was obtained when using PWM at 100% duty cycle. This implies that PWM operates only in the Line of Sight (LoS) region of an underground mines. While, both AM and FM can be deployed beyond the LoS region. Also, beyond 20 m, PWM signal strength begins to fade out and lose power. In non-line-of-sight (NLoS) conditions, the type of modulation scheme deployed becomes inconsequential. The minimum threshold required for RF energy harvesting to be effective is −15 dBm while for communication, the signal strength required is −100 dBm. Hence, NLoS and LoS conditions play pivotal roles.

7.5 Energy replenishment in supercapacitors

We study how effectively the WPT process replenishes energy in three (3) different values of supercapacitors as depicted in Table 5. We connected the VOUT and GND rails

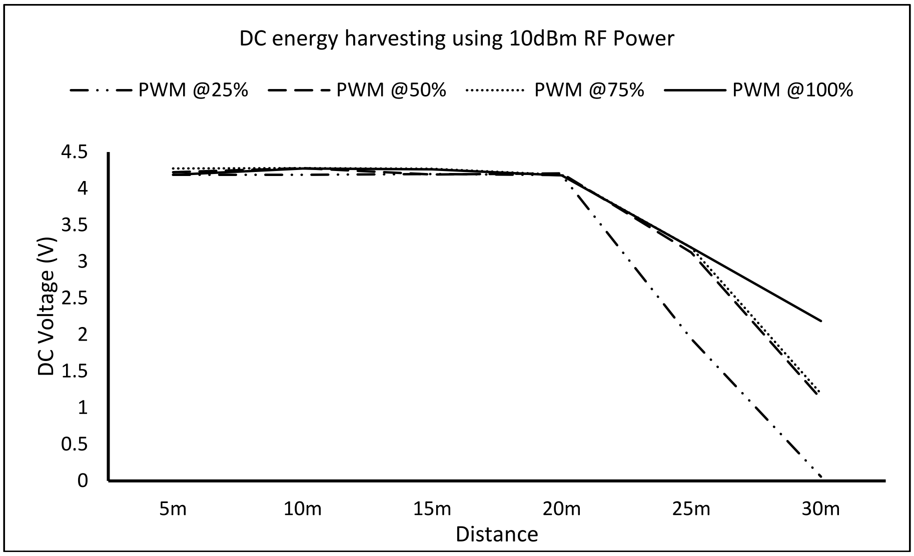

Fig. 10 PWM DC voltage over distance with 10dBm RF power

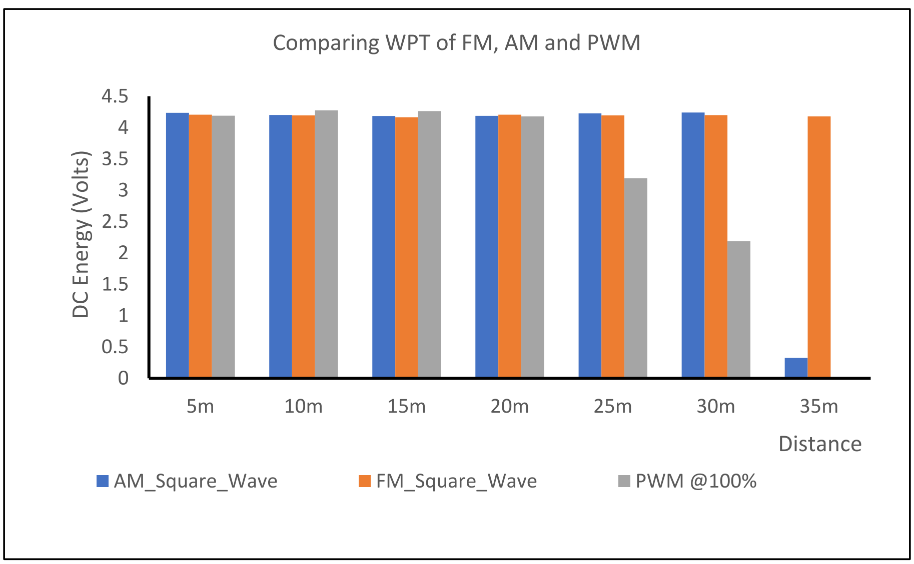

Fig. 11 Comparing AM, FM and PWM DC voltage over distance

of the P21XXCSR-EVB to positive and negative terminals of the various supercapacitors under investigation and measure the rate of voltage charge with the digital oscilloscope. The supercapacitors were partially discharged and were left with limited residual voltages in millivolts. The rate of the charging of the various supercapacitors were logged using the Keysight PathWave BenchVue oscilloscope software for remote control, data logging, and automated testing.

The limitation of the two inbuilt P21XXCSR-EVB capacitors is that their capacitance values are small and thus have limited energy storage capacity. Consequently, the inbuilt capacitors cannot be relied upon to store enough energy to energize microcontroller units for a very long duration. In addition, supercapacitors are widely acclaimed to

Table 5 Supercapacitors charging performance over distances

Distance (Meters)	2.5 Volts 25F			2.7 Volts 100F			5.5 Volts 1F		
	Time (s)	Volt (mV)	Energy (J)	Time (s)	Volt (mV)	Energy (J)	Time (s)	Volt (mV)	Energy (J)
5	120	0.250	1.71125	120	0.37	3.125	120	0.44	0.0968
10	120	0.180	1.12500	120	0.3	1.62	120	0.35	0.06125
15	120	0.100	0.60500	120	0.22	0.5	120	0.24	0.0288
20	120	0.060	0.18000	120	0.12	0.18	120	0.19	0.01805
25	120	0.090	0.08000	120	0.08	0.405	120	0.1	0.005
30	120	0.009	0.00061	120	0.007	0.00405	120	0.01	0.00005
35	120	0.015	0.00005	120	0.002	0.01125	120	0.01	0.00005

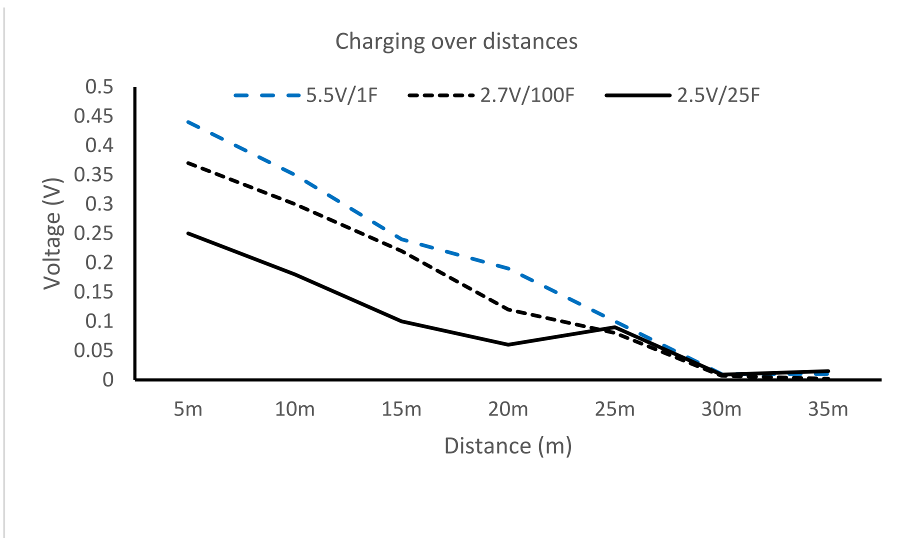

Fig. 12 Illustration of energy harvesting over distance

charge and discharge rapidly. Therefore, providing the needed energy boost for IoT and WSN operations. The energy stored in joules by the various capacitors is derived using Eq. (14):

$$U_C = \frac{1}{2}CV^2 \tag{14}$$

C is the capacitance of the supercapacitor, V is the supercapacitor voltage. Clearly, it could be that 5 V/1F supercapacitor has the fastest rate of charging as could be seen from Table 5 and Fig. 12 respectively. However, the stored energy is minimal and cannot power the Heltec ESP32 SoC MCU used for this study. From the concept of harvested energy storage, 2.7 V/100F stores the highest energy as could be seen from Table 5 and Fig. 13 respectively, however, it takes a lot of time to charge. Hence, we adopted the 2.5 V/25F supercapacitor to power the ESP32 Heltec MCU. Unfortunately, the Heltec ESP32 SoC MCU deployed for this study has a predetermined startup voltage of 3.7 V. Consequently, the chosen 2.5 V/25F was not able to power on the Heltec ESP32 SoC

MCU. This issue was addressed by integrating TPS6109x synchronous boost converter with 2-A switch. This converter generates a stable output voltage that is either adjusted by an external resistor divider or fixed internally on the chip. It provides highly efficient power conversion and can deliver output currents up to 0.5 A at 5 V at a supply voltage down to 1.8 V.

7.6 Perfomance analysis of heltec ESP 32 WiFi BLE + 2.5 V/25F voltage discharge rate

The ESP32 SoC MCU is the bedrock of IoT technology because it provides enabling connectivity for nodes to be connected to the information superhighway. The Heltec ESP32 SoC MCU was programmed using Arduino integrated development environment (IDE) under five (5) different scenarios to determine supercapacitor discharge rate, the current consumption and the energy profiles as shown in Figs. 14, 15 and 16 respectively.

The five (5) different WiFi scenarios include i) the Heltec ESP32 SoC undertaking the role of Access Point (AP) initialization, ii) the AP broadcasting with 5 seconds delay time after initialization, iii) the Heltec ESP32 SoC acting as WiFi station, wakes up, scan for networks with a 20 seconds delay, iv) the Heltec ESP32 SoC connects to AP and obtain the received signal strength indicator (RSSI) value and, v) the Heltec ESP32 SoC obtains the ESP32 IP address to setup its communications link. These processes refer to active mode in MCU SoC configuration. Similarly, the five (5) different Bluetooth Low Energy (BLE) 5.0 scenarios are i) beacon scanner; ii) BLE 5.0 extended scan; iii) BLE 5.0 multiple advertising; iv) BLE 5.0 periodic advertising and v) BLE 5.0 periodic scanning. The 2.5V/25F supercapacitor was charged up to 2.5V and was connected to the TPS6109x synchronous boost converter. The dropout voltage of the TPS6109x synchronous boost converter is 1.8V. Thus, we were able to run the Heltec ESP32 SoC MCU for a period even below the minimum required startup voltage. Average power consumption is the total energy used over a period, while peak power consumption is the maximum instantaneous power drawn, often during startup or high-demand periods. In this study, the focus was on average

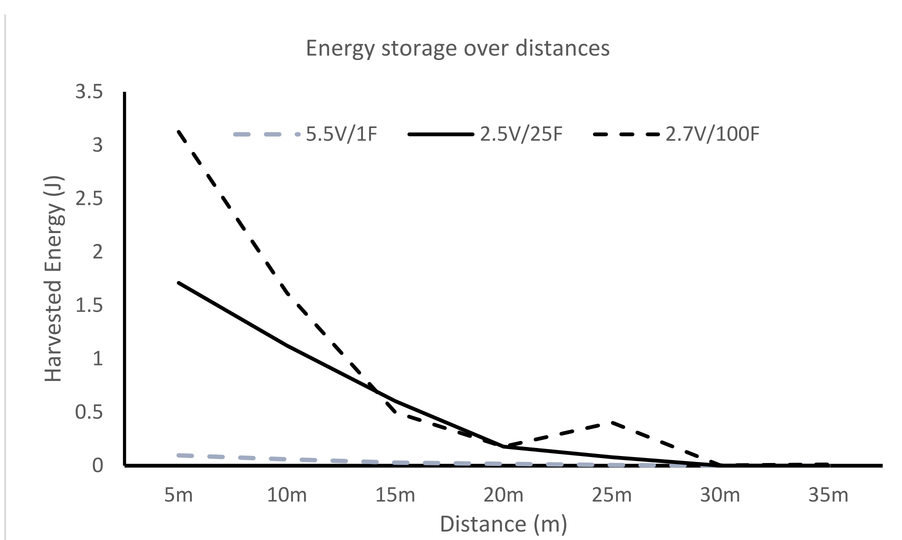

Fig. 13 Illustration of energy storage over distance

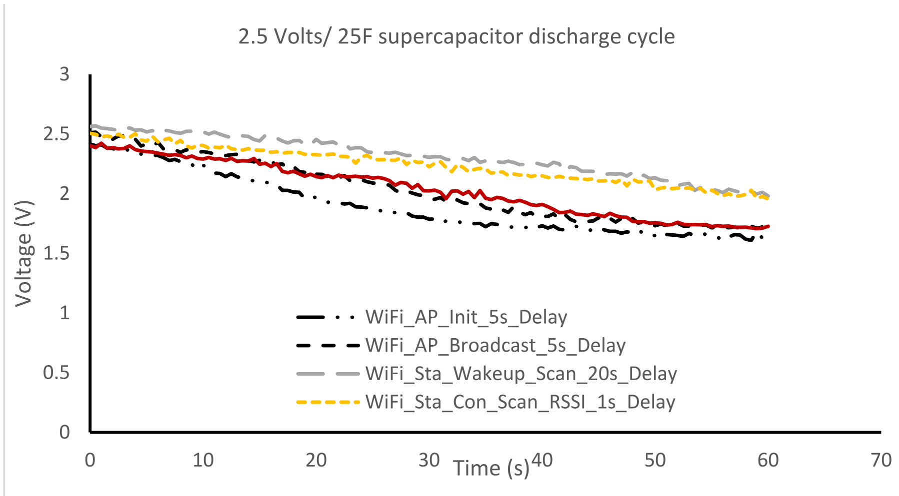

Fig. 14 The Heltec ESP32 SoC MCU WiFi supercapacitor discharge profile

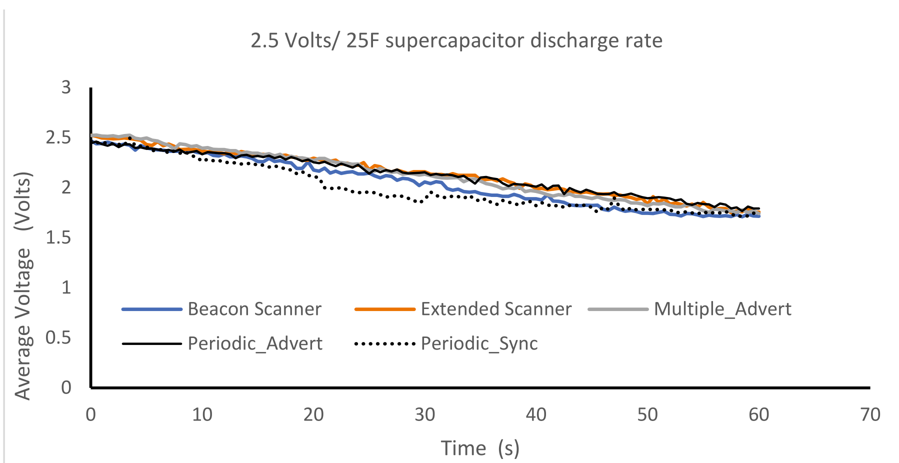

Fig. 15 The Heltec ESP32 SoC MCU BLE 5.0 supercapacitor discharge profile

power consumption. As could be seen from Fig. 14 and 16, when the Heltec ESP32 SoC MCU was configured as APs, both during initialization and transmission, the rate of voltage discharge in volts and current consumption in milliwatts are the highest. Similarly, the least supercapacitor discharge rate occurs when the Heltec ESP32 MCU is configured as WiFi stations. From the BLE 5.0 perspective, the periodic advert scenario contributes minimally to the to the supercapacitor discharge rate while beacon scanner discharges the supercapacitor most rapidly as illustrated in Fig. 15. Figure 16 depicts the power consumption profile of both the BLE 5.0 and WiFi transceivers. It could be seen that WiFi radio consumes the most energy in contrast to BLE 5.0 transceiver module. The different transmission powers of both WiFi and BLE weren't compared because naturally, BLE are designed for short range communication distance and hence their low power consumption attribute.

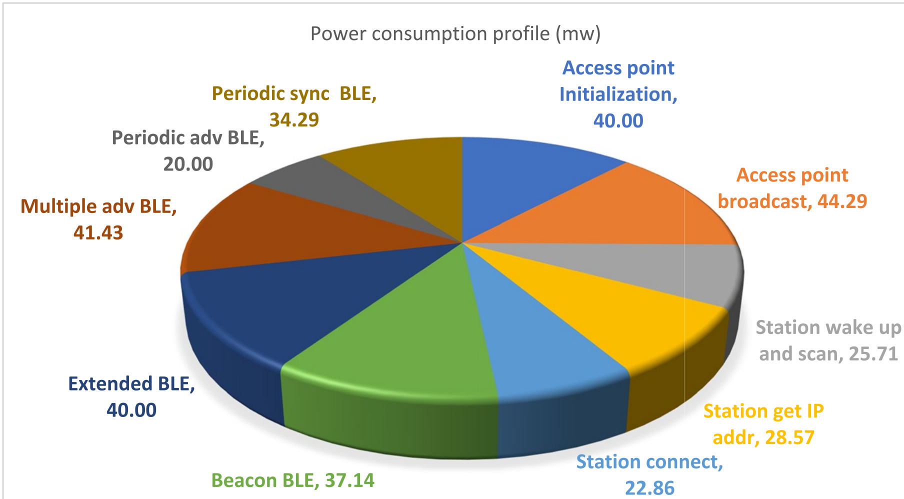

Fig. 16 Heltec ESP32 SoC MCU power consumption profile

7.7 The impact of RTC frequencies on current consumption profile

The Heltec ESP32 was programmed in Arduino IDE to enable Bluetooth and disable it after some milliseconds delay. Then, it will enable and connect to WiFi and disable the WiFi some delay. Finally, it will enable both Bluetooth and WiFi again, and after some milliseconds delay, it will disable ESP32 WiFi and Bluetooth. Using power profiler kit II power measurement tool from Nordic semiconductor, we measured the current consumption of the WiFi and the BLE 5.0 modules in three (3) power modes of i) light sleep; ii) wake up and iii) active modes respectively as shown in Fig. 17. The Nordic Semiconductor Power Profiler Kit II (PPK2) doesn't have a specific calibration procedure, but it's important to ensure the hardware and software are properly set up and connected for accurate measurements. We compared the initial behavior of the Nordic Semiconductor Power Profiler Kit II (PPK2) with a digital oscilloscope before adopting the device. The profile kit II power measurement was configured as power source meter mode which implies that the Heltec ESP32 SoC MCU is powered by the profile profiler kit II. The first scenario is when both the WiFi and BLE5.0 modules are disabled using different RTC values as shown in Fig. 17. Obviously, when the RTC value is 80 MHz, the least current is consumed in contrast to utilizing 240 MHz RTC. Hence, future studies need to adopt lower values of RTC as a strategy to reduce current consumption by Heltec ESP32 SoC MCU. The issue of RTC frequency scaling system on processing speed performance and communication latency is well documented. For instance, lower frequencies (e.g., 80 MHz) has limited timestamp resolution and may introduce timing inaccuracies in time-sensitive applications. Furthermore, a lower-frequency RTC may increase the wake-up delay from sleep modes, affecting responsiveness in interrupt-driven systems. Therefore, in highly latency sensitive networks such as 5G networks and 5G/6G Beyond networks, lower RTC MCU's will be sparsely deployed. From the power profiler, we can observe the energy consumption of light sleep and wakeup is much lower than other parts of the code. Based on the experimental results shown in Fig. 17, it is evident that a higher MCU RTC frequency leads to increased power consumption and reduced energy

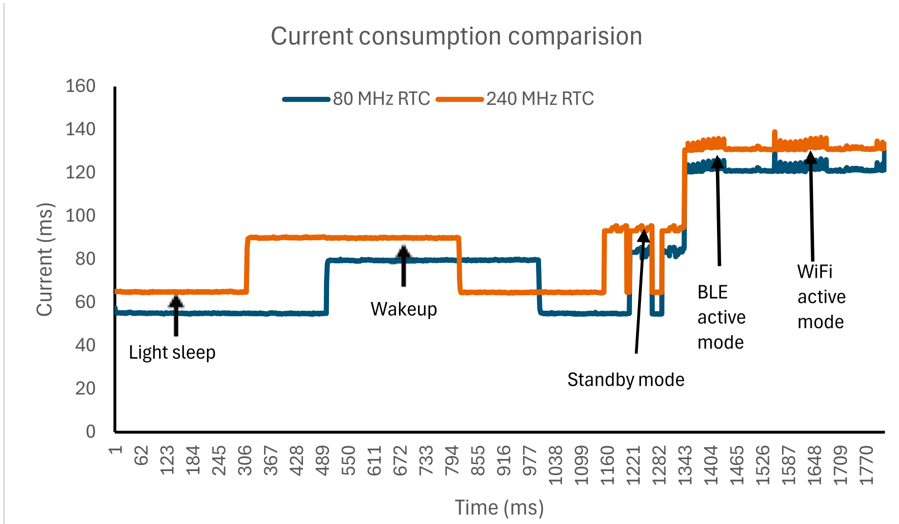

Fig. 17 Baseline current consumption of Heltec ESP32 SoC MCU

efficiency. Power consumption scales proportionally with clock frequency *($P \propto CV^2f$) where* P, C, V, f denotes power, capacitance, voltage and frequency respectively. When the RTC frequency is reduced, the dynamic power consumption decreases linearly. Time sensitive real-time IoT devices such as health monitoring related applications will be driven by high frequency RTC MCUs at the expense of high energy consumption while non time sensitive IoT applications including weather observatory IoT devices will be best served by low RTC frequency scaling. Transient power spikes during module transitions were clearly captured in . Fig. 17.

8 Conclusions

In this paper, we demonstrated that long distance far-field RF energy harvesting is a feasible technology for underground mines IoT deployment for the first time. The long distance far-field RF energy was achieved by integrating external power amplifier into the RF energy harvesting circuitry. Out of the three (3) modulation schemes analyzed, FM is the most promising modulation scheme. Additionally square carrier wave is the most attractive carrier wave between the FM and AM modulation schemes. Furthermore, 100% duty cycle PWM is the least RF power consuming modulation scheme. The limitation of PWM is that it only operates in the LoS region thus limiting the harvestable RF energy. It was also established that Class AB amplifiers consume more DC bias current and power than Class B amplifiers which makes Class AB amplifiers yield longer ranges in harvestable DC energy. Furthermore, a supercapacitor is sufficient to power Heltec ESP32 SoC MCU thus making the realization of IoT technology in underground mines feasible. However, the issue of supercapacitor leakage current needs to be addressed before deployment. It was apparent that WiFi RF modules consume more current and energy than BLE 5.0 RF module.

Abbreviations

LPWAN	Low-power wireless area networks
IoT	Internet of things

RF	Radio frequency
WPT	Wireless power transfer
SoC	System-on-chip
COTS	Commercially off-the-shelf
PA	Power amplifier
EH	Energy harvesting
AM	Amplitude modulation
FM	Frequency modulation
PWM	Pulse width modulation
MCU	Micro controller unit

Acknowledgements
We will recognize funding from the CDC-NIOSH U60 Program, and the use of the laboratory environments provided at Missouri S&T Experimental Mine.

Author contributions
AHK is responsible for conceptualization, methodology and experimental setup. FS undertook data analysis and manuscript formatting.

Funding
This research was funded by the CDC-NIOSH U60 Program.

Availability of data and materials
Data sharing is not applicable to this article as no datasets were generated or analysed during the current study.

Declarations

Competing interest
There are no competing interests in this work.

Received: 19 October 2024 Accepted: 8 August 2025
Published: 5 December 2025

References

1. X. Lin, W. Lu, A framework for optimization on battery cycle life. J. Electrochem. Soc. **165**(14), A3380 (2018)
2. U. Muncuk, K. Alemdar, J.D. Sarode, K.R. Chowdhury, Multiband ambient RF energy harvesting circuit design for enabling batteryless sensors and IoT. IEEE Internet Things J. **5**(4), 2700–2714 (2018)
3. A.M. Zungeru, L.-M. Ang, S. Prabaharan, K.P. Seng, Radio frequency energy harvesting and management for wireless sensor networks. Green Mob. Devices Netw.: Energy Optim. Scav. Tech. **13**, 341–368 (2012)
4. A. Emslie, R. Lagace, P. Strong, Theory of the propagation of UHF radio waves in coal mine tunnels. IEEE Trans. Antennas Propag. **23**(2), 192–205 (1975)
5. A. Ranjan, H. Sahu, P. Misra, Modeling and measurements for wireless communication networks in underground mine environments. Measurement **149**, 106980 (2020)
6. D. Large, L. Ball, A. Farstad, Radio transmission to and from underground coal mines-theory and measurement. IEEE Trans. Commun. **21**(3), 194–202 (1973)
7. R. Nutter, M.D. Aldridge, Status of mine monitoring and communications. IEEE Trans. Ind. Appl. **24**(5), 820–826 (1988)
8. M. Boutin, A. Benzakour, C.L. Despins, Sn. Affes, Radio wave characterization and modeling in underground mine tunnels. IEEE Trans. Antennas Propag. **56**(2), 540–549 (2008)
9. A.E. Forooshani, S. Bashir, D.G. Michelson, S. Noghanian, A survey of wireless communications and propagation modeling in underground mines. IEEE Commun. Surv. Tutor. **15**(4), 1524–1545 (2013)
10. C. Nerguizian, C.L. Despins, S. Affes, M. Djadel, Radio-channel characterization of an underground mine at 2.4 GHz. IEEE Trans. Wireless Commun. **4**(5), 2441–2453 (2005)
11. A. Benzakour, S. Affes, C. Despins, and P.-M. Tardif, Wideband measurements of channel characteristics at 2.4 and 5.8 GHz in underground mining environments, In: *IEEE 60th Vehicular Technology Conference, 2004. VTC2004-Fall. 2004*, 2004, vol. 5, pp. 3595–3599: IEEE
12. W. Farjow, K. Raahemifar, X. Fernando, Novel wireless channels characterization model for underground mines. Appl. Math. Model. **39**(19), 5997–6007 (2015)
13. S. Yarkan, S. Guzelgoz, H. Arslan, R.R. Murphy, Underground mine communications: a survey. IEEE Commun. Surv. Tutor. **11**(3), 125–142 (2009)
14. B. Button, NIOSH Science Blog
15. D. A. Warnakulasuriya, K. Mikhaylov, and O. L. Alcaraz Lopez, Wireless Power Transfer for Bluetooth Low Energy Based IoT Device: an Empirical Study of Energy Performance. In: presented at the 2022 14th International Congress on Ultra Modern Telecommunications and Control Systems and Workshops (ICUMT), 2022
16. S. Gautam, S. Kumar, S. Chatzinotas, B. Ottersten, Experimental evaluation of RF waveform designs for wireless power transfer using software defined radio. IEEE Access **9**, 132609–132622 (2021)
17. J. Janhunen, K. Mikhaylov, J. Petäjäjärvi, M. Sonkki, Wireless energy transfer powered wireless sensor node for green IoT: design, implementation and evaluation. Sensors **19**(1), 90 (2018)

18. A. Benhamou, M. Tellache, S. Hebib, Wireless power transfer system prototype with a wide input power range rectifier and power-optimized waveforms. Microwave Opt. Technol. Lett. **64**(1), 60–66 (2022)
19. J. Eidaks, J. Sadovskis, A. Litvinenko, and D. Pikulins, Experimental Analysis of LoRa Signals Employment for RF Energy Harvesting. In: *2020 IEEE Microwave Theory and Techniques in Wireless Communications (MTTW)*, 2020, vol. 1, pp. 201–205: IEEE
20. B.T. Malik, V. Doychinov, A.M. Hayajneh, S.A.R. Zaidi, I.D. Robertson, N. Somjit, Wireless power transfer system for battery-less sensor nodes. IEEE Access **8**, 95878–95887 (2020)
21. R. Vyas, H. Nishimoto, M. Tentzeris, Y. Kawahara, and T. Asami, A battery-less, energy harvesting device for long range scavenging of wireless power from terrestrial TV broadcasts. In: *2012 IEEE/MTT-S International Microwave Symposium Digest*, 2012, pp. 1–3: IEEE
22. S. Keyrouz, H. Visser, and A. Tijhuis, Ambient RF energy harvesting from DTV stations. In: *2012 Loughborough Antennas & Propagation Conference (LAPC)*, 2012, pp. 1–4: IEEE
23. M. Arrawatia, M. S. Baghini, and G. Kumar, RF energy harvesting system from cell towers in 900MHz band. In: *2011 National Conference on Communications (NCC)*, 2011, pp. 1–5: IEEE
24. I. Chaour, A. Fakhfakh, O. Kanoun, Enhanced passive RF-DC converter circuit efficiency for low RF energy harvesting. Sensors **17**(3), 546 (2017)
25. N. Ayir, T. Riihonen, M. Allen, M.F. Trujillo Fierro, Waveforms and end-to-end efficiency in RF wireless power transfer using digital radio transmitter. IEEE Trans. Microw. Theory Tech. **69**(3), 1917–1931 (2021)
26. G. Charalampidis, A. Papadakis, M. Samarakou, Power estimation of RF energy harvesters. Energy Procedia **157**, 892–900 (2019)
27. D.-K. Ho, I. Kharrat, V.-D. Ngo, T.-P. Vuong, Q.-C. Nguyen, and M.-T. Le, Dual-band rectenna for ambient RF energy harvesting at GSM 900 MHz and 1800 MHz. In: *2016 IEEE International Conference on Sustainable Energy Technologies (ICSET)*, 2016, pp. 306–310: IEEE
28. D. Mishra, S. De, S. Jana, S. Basagni, K. Chowdhury, W. Heinzelman, Smart RF energy harvesting communications: challenges and opportunities. IEEE Commun. Mag. **53**(4), 70–78 (2015)
29. J. Mendoza and A. Sánchez, On the design of a RF Schottky diode rectifier for energy harvesting applications. In: *2018 IEEE International Autumn Meeting on Power, Electronics and Computing (ROPEC)*, 2018, pp. 1–6: IEEE.
30. S. Scorcioni, L. Larcher, A. Bertacchini, L. Vincetti, and M. Maini, An integrated RF energy harvester for UHF wireless powering applications. In: *2013 IEEE Wireless Power Transfer (WPT)*, 2013, pp. 92–95: IEEE.
31. Y. Lu et al., A wide input range dual-path CMOS rectifier for RF energy harvesting. IEEE Trans. Circuits Syst. II Express Briefs **64**(2), 166–170 (2017)
32. M. Stoopman, S. Keyrouz, H.J. Visser, K. Philips, W.A. Serdijn, Co-design of a CMOS rectifier and small loop antenna for highly sensitive RF energy harvesters. IEEE J. Solid-State Circuits **49**(3), 622–634 (2014)
33. G. Papotto, F. Carrara, G. Palmisano, A 90-nm CMOS threshold-compensated RF energy harvester. IEEE J. Solid-State Circuits **46**(9), 1985–1997 (2011)
34. D. Tse, P. Viswanath, *Fundamentals of wireless communication* (Cambridge University Press, Cambridge, 2005)
35. X. Tang, G. Xie, Y. Cui, Self-sustainable long-range backscattering communication using RF energy harvesting. IEEE Internet Things J. **8**(17), 13737–13749 (2021)
36. M.P. Garde, A. Lopez-Martin, J.M. Algueta, R.G. Carvajal, J. Ramirez-Angulo, Class AB amplifier with enhanced slew rate and GBW. Int. J. Circuit Theory Appl. **47**(8), 1199–1210 (2019)
37. J. Tang, J. Lee, J. Roh, Low-power fast-transient capacitor-less LDO regulator with high slew-rate class-AB amplifier. IEEE Trans. Circuits Syst. II Express Briefs **66**(3), 462–466 (2018)
38. A. Far, Class AB amplifier with noise reduction, speed boost, gain enhancement, and ultra low power. In: *2018 IEEE 9th Latin American Symposium on Circuits & Systems (LASCAS)*, 2018, pp. 1–4: IEEE.
39. H. Choi, Class-C linearized amplifier for portable ultrasound instruments. Sensors **19**(4), 898 (2019)
40. R. Goldberg, New products: arbitrary waveform generators deliver output swings up to 24 V. IEEE Instrum. Meas. Mag. **23**(2), 115–119 (2020)
41. S. Hound. [Online]. Available: https://signalhound.com/
42. D. Neunteufel, S. Grebien, H. Arthaber, Indoor positioning of low-cost narrowband IoT nodes: evaluation of a TDoA approach in a retail environment. Sensors **22**(7), 2663 (2022)
43. M. Hua, Y. Zhang, J. Sun, B. Adebisi, T. Ohtsuki, G. Gui, H.C. Wu, H. Sari, Specific emitter identification using adaptive signal feature embedded knowledge graph. IEEE Internet Things J. **11**(3), 4722–4734 (2023)
44. K.H. Anabi, M. Islam, J. Tiang, A quarter-wave Y-shaped patch antenna with two unequal arms for wideband Ultra High Frequency Radio-frequency identification (UHF RFID) operations. Int. J. Phys. Sci. **6**(26), 6200–6209 (2011)
45. A.H. Kelechi et al., The recent advancement in unmanned aerial vehicle tracking antenna: a review. Sensors **21**(16), 5662 (2021)
46. P. P21XXCSR-EVB. *P21XXPowerharvester® Chipset Reference Design Evaluation Board*. Available: https://www.powercastco.com/wp-content/uploads/2021/06/P21XXCSR-EVB-Datasheet-v2.1-1.pdf
47. (2024, 27/07/2024). *WiFi LoRa 32(V3)*. Available: https://heltec.org/project/wifi-lora-32-v3/
48. W. Shang et al., Insight into the self-discharge suppression of electrochemical capacitors: progress and challenges. Adv.Powder Mater. **2**(1), 100075 (2023)

Publisher's Note